JOURNAL OF SOLID STATE CHEMISTRY 70, 108–120 (1987)

The Modulated Structure of $Mo_{2.065}S_3$*

R. DEBLIECK,† J. VAN LANDUYT, D. VAN DYCK,
G. VAN TENDELOO, AND S. AMELINCKX

Rijksuniversitair Centrum Antwerpen (RUCA), Groenenborgerlaan 171, B-2020 Antwerpen, Belgium

Received December 29, 1986; in revised form March 3, 1987

A study by electron diffraction and high-resolution electron microscopy is reported on the modulated structure of $Mo_{2.065}S_3$. This material first structurally characterized by Jellinek was shown by a combined study of electron and X-ray diffraction to present a modulated structure. The present paper reports an analysis of the fine structure of the electron diffraction data which enables the modulated structure to be described in terms of interface modulations. High-resolution electron microscopy images are consistent with the proposed model. © 1987 Academic Press, Inc.

1. Introduction

The structure of molybdenum sulfide ($Mo_{2.06}S_3$) was determined by Jellinek (*1*) and De Jonge *et al.* (*2*). In an earlier paper by some of the present authors the clustering and "phase-ordering" transitions in molybdenum sulfide were reported as derived from an X-ray diffraction study (*3*).

Although the above-mentioned study resulted in a rather detailed structure model in terms of the formation of 4-atom clusters along the zig-zag chains of Mo atoms, the analysis of the electron diffraction patterns enables a description to be made in terms of an interface modulated structure which is consistent with the X-ray results. It is the purpose of the present paper to report this electron diffraction analysis and to relate its results to the previous description.

2. Description of the Basic Structure

Jellinek in 1961 was the first to unravel the basic structure of Mo_2S_3 from a powder sample (*1*). He found a monoclinic unit cell with $a = 0.6092$ nm, $b = 0.3208$ nm, $c = 0.8633$ nm, and $\beta = 102.43°$. All atoms are in the special positions $2(e)$: $\pm(x, \frac{1}{4}, z)$ of the space group $P2_1/m$.

To a first approximation the sulfur atoms form close-packed layers along the b axis, stacked according to the 4H rule (*ABCBCACAB*) (i.e., *chh* stacking sequence). The octahedral interstices between two of the hexagonally stacked layers are all occupied by Mo atoms, whereas the octahedral interstices in the cubic part of the stacking are only half filled. This idealized model is represented schematically in Fig. 1. The empty rows of octahedra are indicated by crosses.

As a result of the partial filling of octahedra, the hexagonal symmetry is destroyed and the resulting crystal structure is mono-

* Dedicated to Dr. Franz Jellinek.

† Present address: DSM Research, PO Box 18, 6160 MD Geleen, The Netherlands.

0022-4596/87 $3.00

Copyright © 1987 by Academic Press, Inc.
All rights of reproduction in any form reserved.

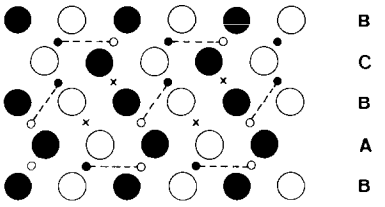

FIG. 1. Idealized structure model based on close packing of sulfur ions. The filled circles indicate atoms at $y = \frac{1}{4}$, whereas the open circles indicate atoms at $y = \frac{3}{4}$. The crosses designate empty octahedral sites. The stacking order is also indicated.

clinic at room temperature. Moreover the Mo atoms are not in the geometrical centers of the octahedra but they are displaced in the direction of one of the octahedron faces in such a way that the neighboring rows of Mo atoms, parallel to the [010] axis (viewing direction of Fig. 1) are connected by a Mo—Mo bond of 0.285 nm thus forming two types of crystallographically independent infinite zig-zag chains running in the [010] direction. The plane of the zig-zag chain of type 1 is approximately parallel to $(\bar{1}01)$ while the plane of the zig-zag chain of type 2 is almost parallel to (001), i.e., the plane of the deformed hexagonal layers of sulfur. The bond length in these chains is only slightly larger than in the pure Mo metal, which is 0.2725 nm.

This basic structure is isotypic with Nb_2Se_3 and Ta_2S_3. De Jonge *et al.* (*2*) confirmed this general picture and refined the basic structure from powder data. The result of this refinement is shown in Fig. 2 where the basic structure is represented and the displacements of atoms from their ideal positions are indicated by arrows.

3. Electron Diffraction Results

3.1. Room Temperature Phase

Six electron diffraction patterns obtained at room temperature along the zones [001], [100], $[\bar{1}11]$, $[\bar{2}31]$, $[10\bar{1}]$, and $[20\bar{1}]$, respectively, are shown in Fig. 3. These can be used to reconstruct the reciprocal lattice. The two most important sections will be discussed in more detail.

3.1.1. The [001] zone pattern. The [001] section of reciprocal space as observed at RT is shown in Fig. 4a and represented schematically in Fig. 4b. The main feature of this section is the doublet of two well-defined superstructure reflections. These pairs are always parallel to b^* and centered in the rectangular mesh of the basic structure reflections. The separation between the two reflections is about 1/17 of b^*. A distortion wave vector $\bar{k}_2$ can be associated with these reflections; its components are $\bar{k}_2 = \frac{1}{2}, \frac{1}{2} - v, 0$ with $v \simeq 0.03$.

Also the Bragg spots of the basic structure acquire two satellites, one on each side situated at distances equal to the separation in the pairs associated with the centers of the meshes. Whereas the arrays of satellites

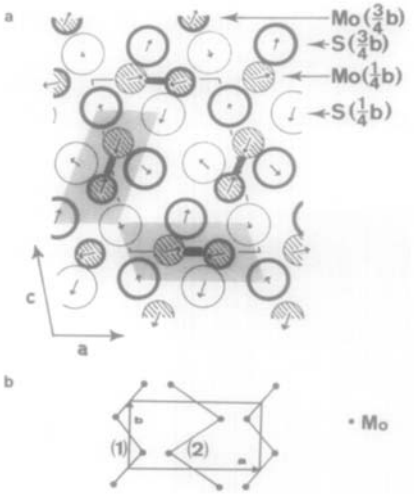

FIG. 2. The basic structure of Mo_2S_3 according to De Jonge *et al.* (*2*). The Mo atoms are indicated as hatched circles. The arrows indicate the displacements from the positions in the ideal lattice shown in Fig. 1 enlarged 2.5 times. The shaded areas indicate the congruent surrounding sulfur configuration of both types of zig-zag chains. These chains are shown in (b) as projected on the (001) plane.

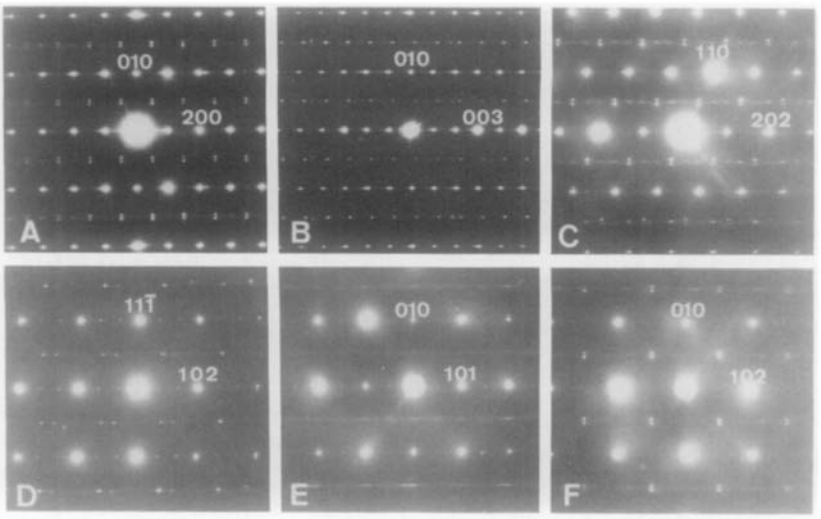

FIG. 3. The electron diffraction pattern of the most interesting sections observed at room temperature: (A) [001] section, (B) [100] section, (C) [$\bar{1}$11] section, (D) [$\bar{2}$31] section, (E) [10$\bar{1}$] section, and (F) [20$\bar{1}$] section.

are shifted over $\frac{1}{2}$ of the interspot distance with respect to the center of the rectangular mesh, the satellites at basic structure reflections are not shifted. In overexposed patterns diffuse streaks are visible, with reinforcements halfway between two neighboring satellite pairs, at $0\ \frac{1}{2}\ 0$. Analysis of several such intersections allows one to conclude that this streak is in fact caused by another pair of satellites associated with the midway positions and oriented along a direction which encloses an angle of 23° with the [001]* axis. This pair of satellites will also be discussed in the following description of the [100] section.

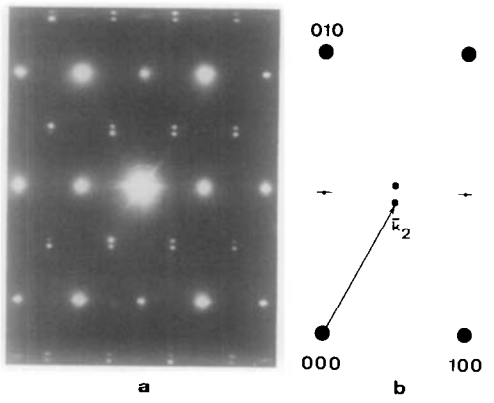

FIG. 4. (a) The diffraction pattern of the [001] zone at RT. (b) Schematic representation of the pattern shown in (a). The distortion wave vector $\bar{k}_2$ is also indicated.

3.1.2. The [100] zone pattern. Figure 5 shows the diffraction pattern along the [100] axis together with its schematic representation. Due to the angle of 23° between the line segment that connects this pair and the [001]* axis, the two reflections are not situated exactly in the zeroth-order plane, which explains the particular intensity variation of these satellites along the [001]* direction. It is also clear from Fig. 5 that the distance between the two neighboring satellite reflections is approximately $\frac{1}{3}c^*$. A distortion wave vector $\bar{k}_1$ can be associated with these reflections:

$$\bar{k}_1 = p, \tfrac{1}{2}, q \qquad \text{with} \quad p = 0.046 \quad q = 0.17$$

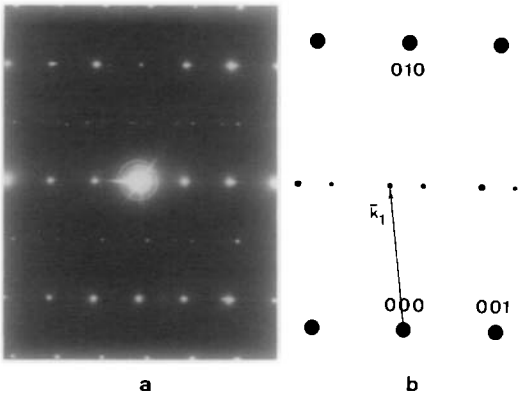

FIG. 5. (a) The diffraction pattern of the [100] zone at RT. (b) Schematic representation of the pattern featuring the distortion wave vector $\bar{k}_1$.

All reflections observed in this section even those corresponding to the basic structure are connected by streaks of diffuse intensity along [001]*.

3.1.3. The [010] zone pattern. It is practically impossible to obtain this zone in the course of a normal electron microscopic investigation of the needle-shaped crystals because it coincides with the needle axis. However, using ultramicrotomy after embedding the needles in a resin, EM specimens can be cut parallel to the (010) planes. The diffraction pattern of a [010] zone thus obtained was used to confirm the reciprocal space model.

3.1.4. The reciprocal space configuration at RT. The different sections of reciprocal space as deduced from the ED patterns have allowed the reconstruction of the reciprocal space configuration which is represented schematically in Fig. 6. Three kinds of satellite arrays occur, two of which have already been discussed in the previous section.

The third kind of satellite array consists of four reflections found at position $\frac{1}{2}\ 0\ 0$ and it features the shifts of the $\bar{k}_1$ and $\bar{k}_2$ arrays. It was discovered by tilting the specimen because these reflections are not in the zeroth-order zone of the most important sections. However, the occurrence of arrays of reflections of type $\bar{k}_1 + \bar{k}_2$ might also be attributed to multiple diffraction phenomena because the presence of arrays of reflections associated with $0\ \frac{1}{2}\ 0$ and $\frac{1}{2}\ \frac{1}{2}\ 0$ implies arrays of reflections associated with $\frac{1}{2}\ n\ 0$ (n = integer).

4. Interpretation of the Electron Diffraction Results as an Interface-Modulated Structure

Structures can be modulated by the periodic occurrence of translation interfaces such as crystallographic shear planes in oxides, antiphase boundaries in ordered alloys, and discommensuration walls. It has been illustrated (*4*) that these structures can be geometrically characterized from electron diffraction patterns by applying the fractional shift method (*5*) which uses geometrical features only of the electron diffraction pattern which are the result of the

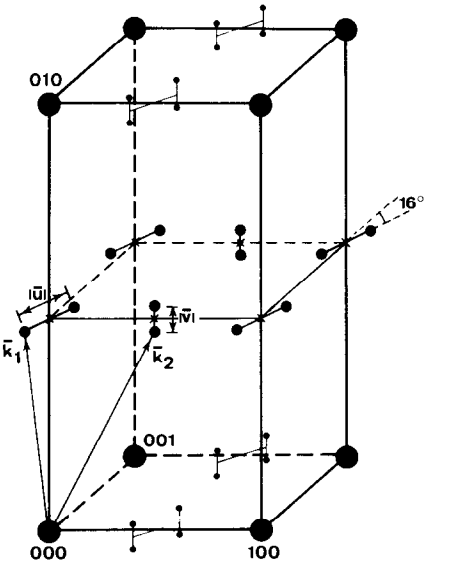

FIG. 6. Reconstruction of reciprocal space at RT as obtained from the electron diffraction analysis ($\phi \simeq 23°$).

periodic occurrence of translation interfaces.

It can be shown in the kinematical approximation for electron diffraction that a periodic modulation in a direction $\bar{n}$ and with period d of translation interfaces characterized by a displacement vector $\bar{R}$ gives rise to satellite reflections at reciprocal lattice positions $\bar{g}$, given by

$$\bar{g} = \bar{H} - (\bar{n}/d)(m - \bar{H} \cdot \bar{R})$$

where m is an integer and $\bar{H}$ is the reciprocal lattice vector of the corresponding basic reflection.

From this expression it appears that the satellite rows $\bar{g}$ are shifted over $\bar{H} \cdot \bar{R}$ with respect to the basic reflection position. The fractional shift $\bar{H} \cdot \bar{R}/d$ measured for three independent reflections $\bar{H}$ yields three equations for the components which is sufficient for the determination of $\bar{R}$ (modulus a lattice vector). It has been shown recently (*13*) that the same diffraction geometry occurs even in cases where the stacking of interface planes is not perfectly periodical but uniform. In this case the satellites are also sharp and d is then the average repeat. This formalism will now be used to interpret the electron diffraction results in terms of displaced blocks of a superstructure. It is, however, necessary to first characterize the superstructure within the blocks as derived from the ED results.

4.1. The Lozenge-Shaped Four-Atom Mo Clusters

It is seen from the diffraction patterns that at sufficiently low temperatures the edges of the unit cell of the basic structure have to be doubled leading to a $2a$, $2b$ "supercell." This superstructure is further modified by long period modulations but before entering into the nature of these modulations the superstructure must first be properly described. Because the sulfur sublattice consists of a rigid close-packed *chh* stacking of atoms it is to be expected that a displacement of Mo atoms is more likely to be at the origin of the superstructure.

Doubling of the b axis by means of small displacements of Mo atoms within the sulfur sublattice can be achieved by clustering of the Mo atoms leading to the formation of four-atom clusters of the type shown in Fig. 7. Such lozenge-shaped four-atom clusters can be compared with the same kind of clusters found in other d-metal compounds: $FeMo_2S_4$, $CoMo_2S_4$ [Guillevic *et al.* (*6*)], $ReSe_2$ [Alcock and Kjekshus (*7*)], Re_2P_5 [Rühl and Jeitschko (*8*)], and Re_6P_{13} [Guerin *et al.* (*9*)].

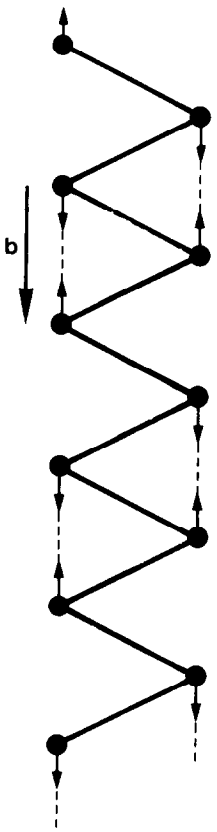

FIG. 7. The formation of lozenge-shaped four-atom clusters in the zig-zag chains.

4.2. *"Phase-Ordering" Transitions*

The formation of the superstructure and of the modulated structure can be described as a "phase-ordering" transition. As the temperature is lowered from the critical temperature, above which it can be assumed that the thermal agitation of the lattice prevents the formation of the clusters, diffuse intensity is observed along planes for which k = const. This clearly indicates a doubling of the repeat distance *along* the chains but in such a way that there is no correlation between the phases of the clustering in adjacent chains.

At lower temperatures the reinforcements in these planes of diffuse intensity develop at the sites where the satellite pairs are to appear later. This indicates a gradual increase of the correlation between adjacent chains. It was found by X-ray analysis that both types of satellite reflections disappear at different temperatures which seems to indicate that two independent one-dimensional systems undergo their own Fermi-level instability-driven transition toward a CDW/PLD. This would suggest that the two types of chains will undergo this kind of transition independently and that both types of structural deformations are to be considered separately.

Because there are no other obvious reasons yet to choose for a model with either coupled or uncoupled chains, both approximations will be considered.

4.3. *The Superstructure*

Prior to the introduction of some long period modulation a superstructure unit cell consistent with the observed intensities must be found. To that purpose it is sufficient to consider the sum of the intensities of two satellite reflections belonging to one cluster at the position around which this cluster is centered. This is based on the fact that in a modulated structure the sum of the intensities of the components of a "split" spot is equal to the intensity of the spot of the unmodulated structure with which the cluster of spots is associated. For the $\bar{k}_1$ and $\bar{k}_2$ reflections these positions are $0\ \frac{1}{2}\ 0$ and $\frac{1}{2}\ \frac{1}{2}\ 0$, respectively.

4.3.1. The "coupled-chain" superstructure unit cell. The superstructure unit cell which must be considered when both types of chains are assumed to be involved simultaneously follows from Fig. 8A where the superlattice positions are represented. The $2a \times 2b \times c$ superstructure unit cell must not be centered and the only way to achieve this for the chains of type 2 (which lie quasicompletely in the *ab* plane) is shown in Fig. 8B. If it is assumed that the oblique chains of type 1 are also subdivided into four-atom clusters, which is justified by the observation that the sulfur environment is identical for both chain types, the complete filling of the unit cell ought to be as shown in Fig. 8B.

The pattern of the clustering in both chains in Fig. 8B is adapted in such a way that the sulfur matrix is the least distorted. This superstructure will be at the origin of the "coupled-chain" interpretation of the modulated structure. It must be noticed that whenever the coupled-chain approximation is correct, the $(\bar{k}_1 + \bar{k}_2)$-type reflections found at $\frac{1}{2}\ 0\ 0$ have a structural origin and are not due to multiple diffraction effects.

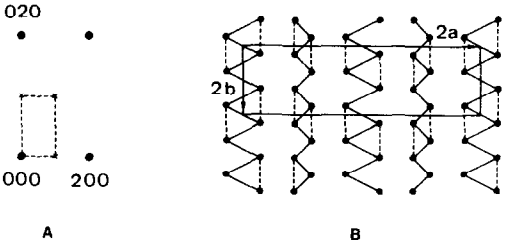

FIG. 8. (A) The relevant intensities for the coupled-chain approximation. (B) The corresponding superstructure unit cell.

4.3.2. The "uncoupled-chain" superstructure unit cells. When independence of the two types of one-dimensional conductor systems is assumed, it follows readily that separated superlattice unit cells will have to be considered for each chain type. Because the $\bar{k}_1$ distortion is more restricted to the *bc* plane it is reasonable to relate it to the chains of type 1 and since the $\bar{k}_2$ distortion is restricted to the *ab* plane it will in the same way be related to the chains of type 2.

(*a*) *The $\bar{k}_1$ superstructure unit cell.* According to the position of the $\bar{k}_1$ satellites shown in Fig. 9A an $a \times 2b \times c$ superstructure unit cell must be considered and the only such unit cell possible is shown in Fig. 9. It involves, as stated before, only the chains of type 1 and shows no doubling of the lattice period along *a*. The chains parallel to the $(\bar{1}01)$ planes are not shown since they are independently implied by the $\bar{k}_2$ distortion.

(*b*) *The $\bar{k}_2$ superstructure unit cell.* Obviously the clusters in the chains of type 2 should be arranged in a centered $2a \times 2b \times c$ unit cell according to the position of the $\bar{k}_2$ satellites shown in Fig. 10A. The only possible configuration involving only the clusters of chains of type 2 is represented in Fig. 11B. Since the chains parallel to the (001) planes are independently implied by the $\bar{k}_1$ distortion they are not shown.

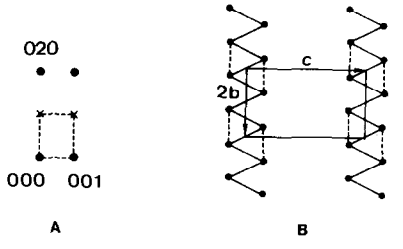

FIG. 9. (A) The relevant intensities for the coupled-chain approximation. (B) The corresponding superstructure unit cell.

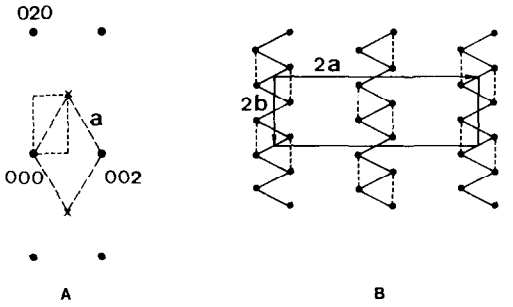

FIG. 10. (A) The superlattice positions for the $\bar{k}_2$ satellites. (B) The corresponding centered superstructure unit cell.

4.4. The Possible Chain Defects Causing Planar Defects

The Mo clusters along a given zig-zag chain can form with four different phases since there are four atoms per cluster. When it is assumed that clustering starts at two different points of the chain either no, one, two, or three "singular" molybdenum atoms are left over and the relative phases of the two ends of the chain are then 0, $\pi/2$, π, $3\pi/2$, respectively.

These possible chain defects are depicted in Fig. 11. It is clear that when the phase is $\pi/2$ or $3\pi/2$, the clusters will be oriented differently on both sides of the chain defect, whereas in the remaining cases they

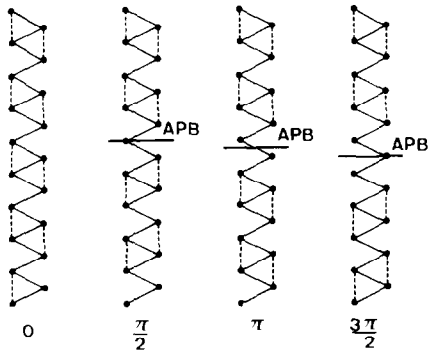

FIG. 11. The possible defects in the Mo-chain clustering.

are oriented in the same way. If either of these defects occurs in neighboring chains at sites located in a planar interface a planar APB will result.

4.5. The Coupled-Chain Modulated Structures

The $\bar{k}_1$ modulated structure. The line segment connecting the two $\bar{k}_1$ satellite reflections is to a rough approximation parallel to c^*; we shall thus assume to a first approximation that the normal to the APBs is parallel to c^*; hence, these interfaces are parallel to the (001) planes. The average distance between the APBs d is then approximately 2 to 3 d_{001}, whereas the displacement vector can be obtained from the observed fractional shifts $\bar{g} \cdot \bar{R}_1^c$ which are indicated in Table I.

The reciprocal lattice vectors are referred to the superstructure unit cell coordinates. It is readily found that $\bar{R}_1^c = [\frac{1}{2}\ \frac{1}{2}\ 0]$ or equivalent. One interface of this nature is shown in Fig. 12. The periodic repetition of the interface leads to the modulated superstructure. The orientation anomaly (i.e., $a,c^* \simeq 30°$) can according to Amelinckx (*5*) be explained in second order by an average orientation of the defect plane due to systematic ledging (i.e., a shift parallel with (001)). Probably this systematic ledging is not perfectly parallel in successive APBs which may also explain why the second-order reflection is never observed.

Because the separation between successive APBs lies between two and three superstructure unit cells, the diffraction pattern must exhibit streaks with reinforcements at the position of the $\bar{k}_1$ satellites corresponding with the average separation as it is clearly observed in the [100] zone patterns.

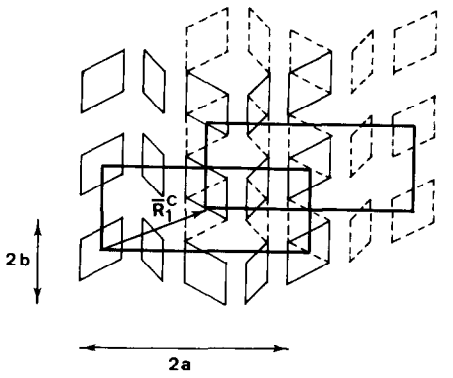

FIG. 12. Defect plane with $\bar{R}_1^c = [\frac{1}{2}\ \frac{1}{2}\ 1]$. The dependent-chain $\bar{k}_1$ modulated structure shows such an APB two to three periods along c. The dashed chains represent a lower parallel (001) plane.

The $\bar{k}_2$ modulated structure. Because $\bar{v}$ is parallel with the b^* axis and because $|\bar{v}|$ is equal to 1/17 b^*, the normal to the APBs responsible for the $\bar{k}_2$ modulation will be along b^* and the separation will be approximately 17 basic structure unit cells. The displacement vector $\bar{R}_2^c$ can again be calculated from the observed fractional shifts $\bar{g}_i\bar{R}_2^c$ gathered in Table II.

It is again readily found that $\bar{R}_2^c = \frac{1}{2}$ [1 0 0] or equivalent. The $\bar{k}_2$ satellite reflections can thus be interpreted as resulting from a set of parallel APBs perpendicular to [010] and at a distance 17b apart. The much weaker higher-order satellite reflections suggest that this separation is only an

TABLE I

$\bar{g}_i$	$\bar{g}_i \cdot \bar{R}_1^c$
010	$\frac{1}{2}$
100	$\frac{1}{2}$
011	$\frac{1}{2}$

TABLE II

$\bar{g}_i$	$\bar{g}_i \cdot \bar{R}_2^c$
100	$\frac{1}{2}$
010	1
110	$\frac{1}{2}$
001	1

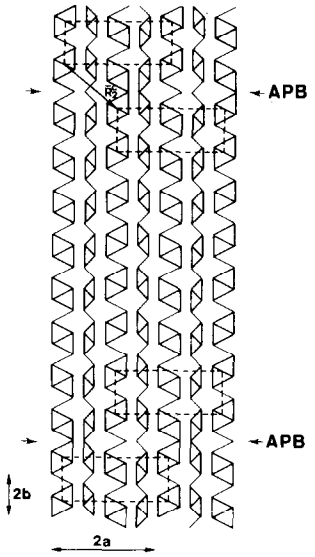

FIG. 13. The $\bar{k}_2$ modulated structure in the coupled-chain approximation. The displacement vector at APBs is $\bar{R}_2^c = \frac{1}{2}[120]$.

average spacing. For instance, it could be a succession of 16*b* and 18*b* (i.e., the superstructure allows only even values). Van Dyck *et al.* (*10*) pointed out that the intensities of the higher-order satellite reflections decrease drastically with decreasing correlation between the widths of adjacent periods. The resulting modulated structure associated with $\bar{k}_2$ in the coupled chain approach is depicted in Fig. 13.

4.6. The Uncoupled-Chain-Modulated Structures

The $\bar{k}_1$ modulated structure. It will again be assumed in a first approximation that $\bar{u}$ is

TABLE III

$\bar{g}_i$	$\bar{g}_i\bar{R}_1^u$
010	$\frac{1}{2}$
001	0
011	$\frac{1}{2}$
110	$\frac{1}{2}$

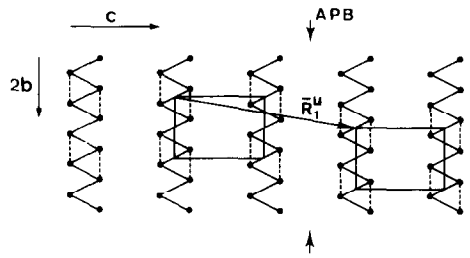

FIG. 14. The $\bar{k}_1$ modulated structure in the uncoupled-chain approach features APBs with displacement vector $\bar{R}_1^u = \frac{1}{2}[0\ 1\ 4]$.

parallel to c^* so that the APBs with displacement vector $\bar{R}_1^u$ will be parallel with the (001) planes. The average distance between the APBs remains between 2 and 3 d_{001} and the displacement vector can be calculated from the fractional shifts $\bar{g}_i\bar{R}_1^u$ shown in Table III where the reciprocal lattice vectors $\bar{g}_i$ are referred to the already derived commensurate superstructure. It is readily found that $\bar{R}_1^u = [0\ \frac{1}{2}\ 0]$ or equivalent. The periodic repetition of this APB leads to the modulated structure shown in Fig. 14.

The orientation anomaly of the $\bar{k}_1$ cluster can be explained by systematic ledging as it is represented schematically in Fig. 15. It is

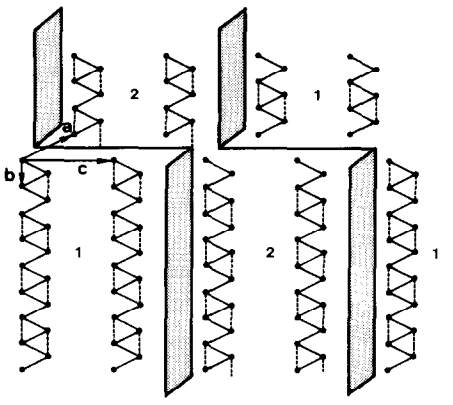

FIG. 15. The systematic ledges of the APBs causing the orientation anomaly. The distance between the APBs is 2*c*. The two occurring phases of clustering are indicated as (1) and (2).

TABLE IV

$\bar{g}_i$	$\bar{g}_i\bar{R}_2^u$
100	$\frac{1}{2}$
010	$\frac{1}{2}$
001	1
110	1

clearly seen that the APB "jogs" from the upper (100) layer to the next (partially hidden) (100) layer.

The $\bar{k}_2$ modulated structure. The APB parallel with the (010) planes and separated by approximately 8 to 9 centered superstructure unit cells have a displacement vector $\bar{R}_2^u$ which can be deduced from the fractional shifts $\bar{g}_i\bar{R}_2^u$ given in Table IV. The reciprocal lattice vectors $\bar{g}_i$ refer to the primitive superstructure unit cell. It then follows that $\bar{R}_2^u = [\frac{1}{2}\ \frac{1}{2}\ 0]$ expressed in primitive superstructure unit cell coordinates. Expressed in terms of the centered $2a, 2b, c$ superstructure unit cell one finds $\bar{R}_2^u = [\frac{1}{2}, 0\ 0]$ (or $[0, \frac{1}{2}, 0]$ which is equivalent). It is clear that the periodic repetition of this APB leads to the modulated structure shown in Fig. 16, together with the interface representation of the modulated structure with the sharp stepwise phase-front evolution (phase jump) of the displacement field across the APB, the average wave vector $\langle\bar{k}_2\rangle$ of the modulated structure is shown. This average for n blocks of the basic structure unit cells with one phase jump every n blocks makes an angle $\theta_{\bar{k}_2}$ with the b axis given by

$$\tan\theta_{\langle\bar{k}_2\rangle} = \frac{n+1}{n}\frac{b}{a}$$

and when $n = 17$,

$$\text{tg}\,\theta_{\langle\bar{k}_2\rangle} = \frac{18}{17}\frac{b}{a}$$

$$\theta_{\langle\bar{k}_2\rangle} = \text{Arctan}\left(\frac{18}{17}\frac{b}{a}\right) = 29.14°$$

which has to be compared with the "undistorted" $\bar{k}_2$:

$$\theta_{\langle\bar{k}_2\rangle} = \text{Arctan}\left(\frac{b}{a}\right) = 27.77°$$

and the deviation

$$\delta\theta_{\bar{k}_2} = \theta_{\langle\bar{k}_2\rangle} - \theta_{\bar{k}_2} = 1.37°$$

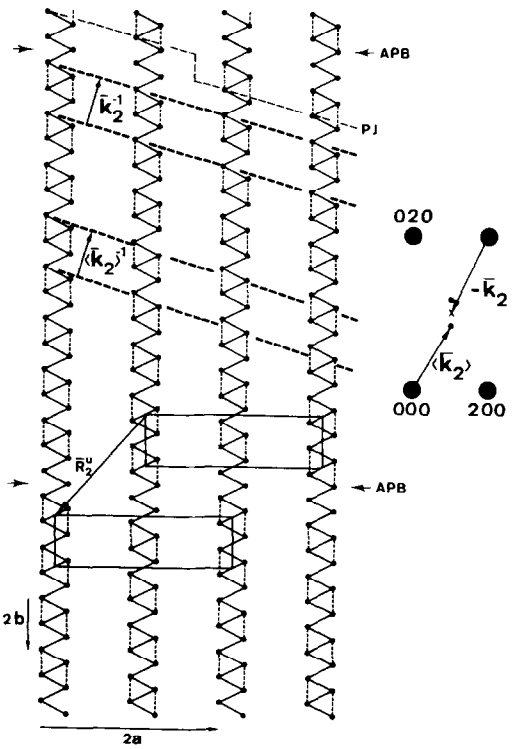

FIG. 16. The $\bar{k}_2$ modulated structure in the uncoupled-chain approximation. The $2a \times 2b$ superstructure unit cell is indicated. The displacement vector between neighboring blocks separated by an APB is also indicated. The phase jump (PJ) is shown in the upper part and the relation between $\bar{k}_2$ and $\langle\bar{k}_2\rangle$ becomes clear when comparing with the diffraction pattern representation (right).

is within the experimental error equal to the deviation determined from the diffraction patterns ($\simeq 1.4°$ ($\pm 0.2°$)).

In order to demonstrate with an example the equivalence of the deformation and interface-modulation description of a modulated structure, the clustering in a Mo chain is modulated one-dimensionally by a harmonic sinusoidal displacement field. The phase ordering between neighboring chains is such that each chain is in antiphase with its neighbor. It is obvious from Fig. 17 that this structure will feature discommensurations parallel to the (010) planes and hence it differs only from the pure interface-modulated structure shown in Fig. 16 in its width of the discommensuration.

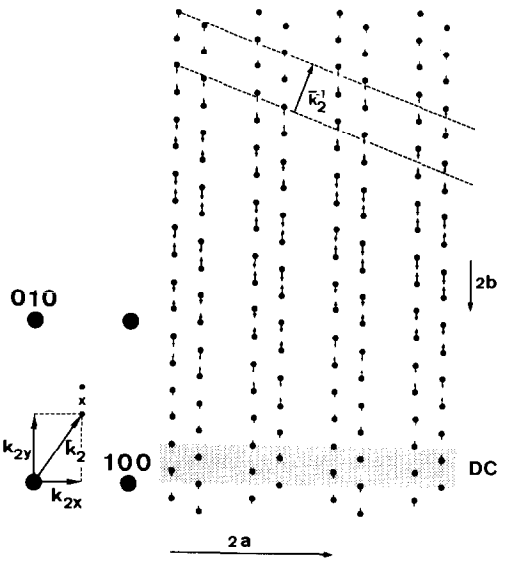

FIG. 17. The wave vector $\bar{k}_2$ in the deformation description can be thought of as decomposed into two components as shown in the left part of the figure. Within the chains, the displacements are assumed to be sinusoidally modulated according to $\delta_y = A \sin(2\pi k_{2y} y)$ with $k_{2y} = 0.47$ (i.e., $\frac{1}{2} - |\bar{v}|/2$). The chains are in antiphase according to the modulation $\delta_x = A \sin 2\pi k_{2x} x$ where $k_{2x} = 0.5$, which is the wave-vector component along [100]*. The resulting structure features discommensurations parallel to the (010) planes every 17 Mo atoms. One such discommensuration is indicated (DC).

5. Direct Imaging of the Modulated Structure

High-resolution imaging of the modulated structure is not straightforward because the satellites are always very weak and the ribbons are rarely very thin. Attempts to image the $\bar{k}_1$ modulated structure were unsuccessful because the satellites are not located exactly in the [100] zone which is the crystal habit, and because these satellites easily fade out due to heating.

The $\bar{k}_2$ modulated structure is more stable and dark-field microscopy selecting both satellites around the $\frac{1}{2}\ \frac{1}{2}\ 0$ position (see Fig. 4) reveals the modulation present on the whole ribbon. No domain fragmentation nor discommensuration dislocations as in $TaSe_2$ (*11*) or $NbTe_4$ (*12*) were observed (see Fig. 18a). On this image the distortion which gives rise to the $\bar{k}_2$ reflections is observed as rather broad lines which can be associated with a continuous deformation or an abrupt phase change. Also the bright-field high-resolution image in Fig. 18b obtained with a large objective aperture to include basic as well as satellite reflections in a [001] section shows a large continuous modulation rather than a sharp interface modulated structure.

It is not possible to conclude from the geometry of the diffraction pattern whether the phase slip is taking place along sharp interfaces or is gradual along discommensurations. The fractional shift method cannot provide this information. However, the images suggest that the phase slip occurs in rather broad domain walls.

These domain walls are not always strictly confined to c planes, as a result of systematic relative shifts between adjacent chains they may be inclined, giving rise to the observed orientation anomalies in the diffraction pattern.

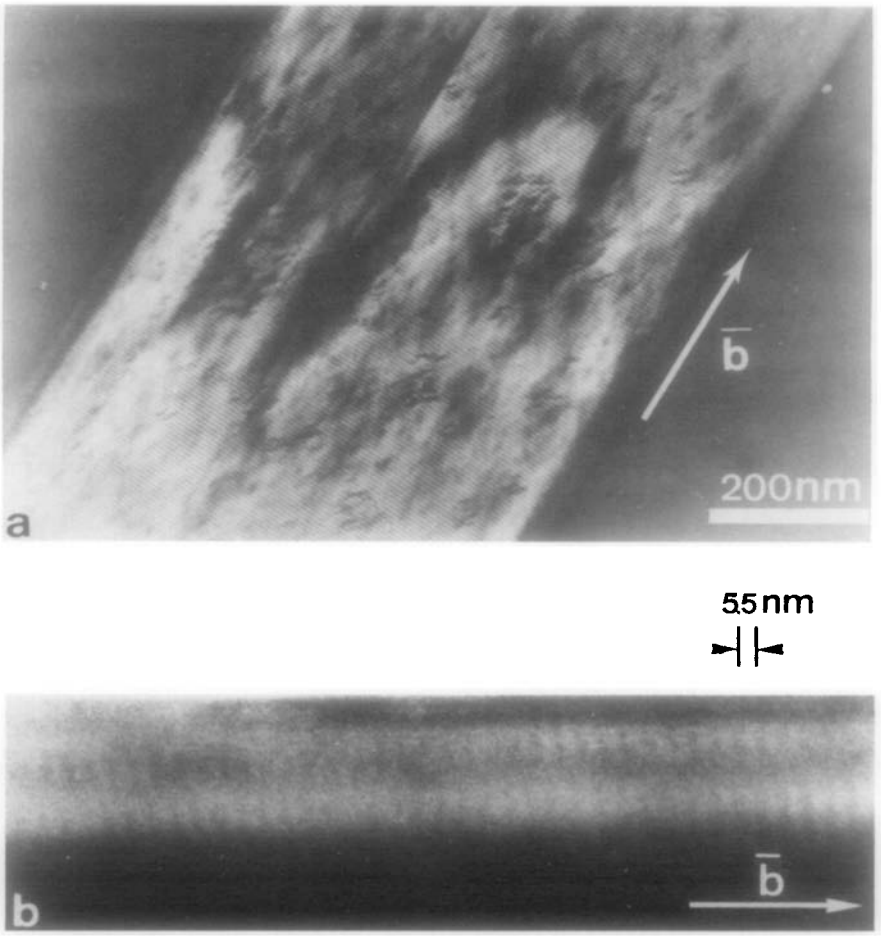

FIG. 18. (a) Dark-field image of the superstructure observed in one cluster of $\bar{k}_2$ reflections. A 5.5-nm period is visible in a direction perpendicular to $\bar{b}$. (b) Bright-field high-resolution image along the [001] zone. A Moiré-like continuous modulation is observed.

6. Concluding Remarks

An analysis of the fine structure of the electron diffraction data of the modulated structure in $Mo_{2.065}S_3$ made a description in terms of interface modulations possible. The superstructure and the displacement vector of the interfaces were deduced from a geometrical interpretation of the diffraction patterns (method of fractional shifts). Both the case of coupled and of noncoupled Mo chains were considered.

High-resolution electron microscopy results confirm the presence of a rather continuous modulation which is not in contradiction to the interface-modulation description.

Acknowledgments

Thanks are due to Professor Jellinek for his stimulating discussions and to the research group in R.U. Groningen, in particular Dr. G. Wiegers, for fruitful collaboration on this subject.

References

1. F. JELLINEK, *Nature* **192,** 1065 (1961).
2. R. DE JONGE, T. J. A. POPMA, G. A. WIEGERS, AND F. JELLINEK, *J. Solid State Chem.* **2,** 188 (1970).
3. R. DEBLIECK, G. A. WEIGERS, K. BRONSEMA, D. VAN DYCK, G. VAN TENDELOO, J. VAN LANDUYT, AND S. AMELINCKX, *Phys. Status Solidi A* **77,** 249 (1983).
4. J. VAN LANDUYT, R. DE RIDDER, R. GEVERS, AND S. AMELINCKX, *Mater. Res. Bull.* **5,** 353 (1970).
5. S. AMELINCKX, *AIP Conf. Proc.* **53,** 102 (1979).
6. J. GUILLEVIC, J. Y. MAROUILLE, AND D. GRANDJEAN, *Acta Crystallogr.* **B30,** 111 (1974).
7. N. W. ALCOCK AND A. KJEKSHUS, *Acta Chem. Scand.* **19,** 79 (1965).
8. R. RÜHL AND W. JEITSCHKO, *Inorg. Chem.* **21,** 1886 (1982).
9. R. GUERIN, M. POTEL, AND M. SERGENT, *Mater. Res. Bull.* **B14,** 133 (1974).
10. D. VAN DYCK, C. CONDE, AND S. AMELINCKX, *Phys. Status Solidi A* **56,** 327 (1979).
11. K. K. FUNG AND J. W. STEEDS, *Phys. Rev. Lett.* **45,** 1696 (1980).
12. J. MAHY, J. VAN LANDUYT, S. AMELINCKX, K. D. BRONSEMA, AND S. VAN SMAALEN, *J. Phys. C* **19,** 5049 (1986).
13. D. VAN DYCK, J. MAHY, AND S. AMELINCKX, to be published.